



Liu, Y., Horseman, T., Wang, Z., Arafat, H. A., Yin, H., Lin, S. and He, T. (2022) Negative pressure membrane distillation for excellent gypsum scaling resistance and flux enhancement. *Environmental Science and Technology*, 56(2), pp. 1405-1412.

(doi: [10.1021/acs.est.1c07144](https://doi.org/10.1021/acs.est.1c07144))

This is the Author Accepted Manuscript.

There may be differences between this version and the published version. You are advised to consult the publisher's version if you wish to cite from it.

<https://eprints.gla.ac.uk/261961/>

Deposited on: 28 April 2022

1
2
3
4
5
6
7
8
9
10
11
12
13
14
15
16
17
18
19
20
21
22
23
24
25
26
27
28
29

Negative Pressure Membrane Distillation for Excellent Gypsum Scaling Resistance and Flux Enhancement

manuscript submitted to

Environmental Science & Technology

Yongjie Liu^{a,b}, Thomas Horseman^c, Zhangxin Wang^{d,e}, Hassan A. Arafat^b, Huabing Yin^f,
Shihong Lin^{c,g,*}, Tao He^{a,*}

- a. Shanghai Advanced Research Institute, Chinese Academy of Sciences, Shanghai 201210, China
- b. Center for Membrane and Advanced Water Technology, Khalifa University, Abu Dhabi, United Arab Emirates
- c. Department of Chemical and Biomolecular Engineering, Vanderbilt University, Nashville, Tennessee 37235-1831, United States
- d. Key Laboratory for City Cluster Environmental Safety and Green Development of the Ministry of Education, Institute of Environmental and Ecological Engineering, Guangdong University of Technology, Guangzhou, 510006, China
- e. Guangdong Provincial Key Laboratory of Water Quality Improvement and Ecological Restoration for Watershed, Institute of Environmental and Ecological Engineering, Guangdong University of Technology, Guangzhou, 510006, China
- f. School of Engineering, University of Glasgow, Glasgow, G12 8LT, UK
- g. Department of Civil and Environmental Engineering, Vanderbilt University, Nashville, Tennessee 37235-1831, United States

*Corresponding authors:

Shihong Lin shihong.lin@vanderbilt.edu Tao He het@sari.ac.cn

30 **ABSTRACT**

31 Membrane distillation (MD) has the potential to become a competitive technology for managing
32 hypersaline brine, but not until the critical challenge of mineral scaling is addressed. The state-of-
33 the-art approach for mitigating mineral scaling in MD involves the use of superhydrophobic
34 membranes that are difficult to fabricate and commercially unavailable. This study explores a
35 novel operational strategy, namely negative pressure direct contact membrane distillation (NP-
36 DCMD), that can minimize mineral scaling with commercially available hydrophobic membranes,
37 and at the same time enhance water vapor flux substantially. By applying a negative gauge pressure
38 on the feed stream, NP-DCMD achieved prolonged resistance to CaSO_4 scaling and a dramatic
39 vapor flux enhancement up to 62%. The exceptional scaling resistance is attributable to the
40 formation of a concave liquid-gas under negative pressure that changes the position of the water-
41 air interface to hinder interfacial nucleation and crystal growth. The substantial flux enhancement
42 is caused by the reduced molecular diffusion resistance within the pores and the enhanced heat
43 transfer kinetics across the boundary layer in NP-DCMD. Achieving substantial performance
44 improvement in both scaling resistance and vapor flux with commercial membranes, NP-DCMD
45 is a significant innovation with vast potential for practical adoption due to its simplicity and
46 effectiveness.

47 **Keywords:** membrane distillation; negative pressure; scaling resistance; water-air interface; slip
48 boundary

49 **Synopsis:** Negative feed stream pressure mitigates gypsum scaling and enhances vapor flux in
50 direct contact membrane distillation.

51 INTRODUCTION

52 Membrane distillation (MD) is a thermally driven desalination process where a
53 microporous hydrophobic membrane acts as a physical barrier of direct liquid transfer between hot
54 feed and cold distillate streams.¹ Due to the transmembrane temperature gradient-induced vapor
55 pressure gradient, water vapor transports through the membrane pores from the feed to the distillate.
56 As vapor pressure is weakly dependent on feed salinity, MD is an attractive process for hypersaline
57 brine treatment where the osmotic pressure requirements make reverse osmosis (RO)
58 inapplicable.² Furthermore, the ability to power MD with low-grade heat, such as solar or
59 geothermal energy and waste heat from industrial processes, makes it attractive from a
60 sustainability perspective. Compared to conventional thermal desalination processes like multi-
61 stage flash and multi-effect distillation, the compact modular design of MD makes it more
62 competitive for distributed brine treatment and integration with other modular brine treatment
63 processes.^{3,4}

64 Nevertheless, a big challenge of MD, especially in treating hypersaline brine, is mineral
65 scaling (also referred to as inorganic fouling).⁵⁻⁷ Scaling occurs when the feed solution is
66 concentrated beyond its solubility limit, which results in mineral precipitation. The precipitated
67 minerals block the membrane pores and reduce the membrane's water vapor permeability. Scaling
68 by gypsum, silica, calcite, sodium chloride, and mixed salt feed solutions have been investigated.
69 ⁸⁻¹³ Among different types of scalants, gypsum is one of the most challenging and widely studied
70 scalants due to its practical relevance and its low and pH insensitive solubility, i.e., scaling by
71 gypsum cannot be mitigated by merely adjusting the pH of the feed solution as in the case of
72 mitigating calcite scaling.^{8, 14, 15}

73 In a scaling process, nucleation of mineral precipitates typically occurs via two concurrent
74 pathways: 1) in the bulk solution, and 2) heterogeneously on the membrane surface.¹⁶⁻¹⁸ On one
75 hand, precipitates that nucleate in the bulk solution may deposit on the membrane surface and
76 block the pores, resulting in flux decline and providing potential growth sites for further mineral
77 growth. On the other hand, precipitates that nucleate in the membrane pores (near the surface) not
78 only block the pores but may eventually lead to membrane pore deformation due to crystallization
79 pressure within the membrane pores. Pore deformation often results in membrane pore wetting as
80 the liquid entry pressure decreases and the crystals create a pathway for direct liquid feed
81 permeation through the membrane.¹⁴ Both the fouling and wetting mechanisms of scaling can
82 result in complete process failure.¹⁷

83 As membrane wetting can be mitigated using omniphobic membranes,¹⁹⁻²¹ recent studies
84 have also shown that superhydrophobic membranes are effective for scaling mitigation.
85 Superhydrophobic membranes, sometimes referred to as slippery membranes due to their low
86 sliding angles with water, can delay the onset of mineral scaling or even nearly eliminate scaling
87 in some cases, depending on the scaling species and operation mode.^{8, 11, 15, 22, 23} For example,
88 superhydrophobic membranes alone were shown to dramatically delay scaling by gypsum and
89 entirely inhibit scaling by sodium chloride.^{11, 14} When combining superhydrophobic membranes
90 and operational innovations synergistically, even gypsum scaling can be inhibited altogether.^{23, 24}
91 Furthermore, superhydrophobic membranes have significantly reduced mineral scaling with real
92 industrial wastewaters such as cooling tower blowdown from power plants.^{8, 25} The scaling
93 resistance can be attributed to the low adhesion, air-filled, superhydrophobic surface that 1)
94 reduces liquid-membrane contact area available for crystal deposition or growth, 2) has a low
95 surface energy and thus a low propensity for heterogeneous nucleation, and 3) introduces a slip

96 boundary condition that inhibits concentration polarization and long residence time for crystal
97 growth and deposition.¹⁷ In most studies, commercial hydrophobic membranes, which lack all
98 these features, were used as a reference for comparison and have consistently shown very poor
99 scaling resistance.

100 However, superhydrophobic membranes are not commercially available and the
101 fabrication thereof adds cost and complexity to the manufacturing process. Additionally, the
102 fabrication of superhydrophobic membranes often involves the use of per-fluorinated compounds
103 and nanoparticles coating, which raises environmental and health concerns to both manufacturing
104 and using such membranes.^{15, 26-32} Therefore, despite the great promise superhydrophobic
105 membranes have shown to attain scaling resistance, it is practically much more appealing if scaling
106 resistance can be achieved with conventional and commercially available hydrophobic membranes.

107 In this study, we show that excellent gypsum scaling resistance and flux enhancement can
108 be achieved using conventional commercial hydrophobic membranes with a novel operation mode,
109 namely negative pressure direct contact membrane distillation (NP-DCMD). Unlike conventional
110 DCMD, in which the feed pump is placed upstream of the feed channel pushing the feed water
111 into the MD cell (or module), the feed pump in NP-DCMD is placed downstream of the feed
112 channel withdrawing water from the MD cell (or module). Consequently, the feed stream in
113 conventional DCMD has a positive gauge pressure (i.e., relative to atmospheric pressure), whereas
114 the feed stream in NP-DCMD has a negative gauge pressure. By performing DCMD experiments
115 with both positive and negative feed (gauge) pressures, we systematically compare the scaling
116 resistance and water vapor flux in these two configurations. We also perform mass and heat
117 transfer modeling to elucidate the mechanism of vapor flux enhancement achieved by NP-DCMD.

118

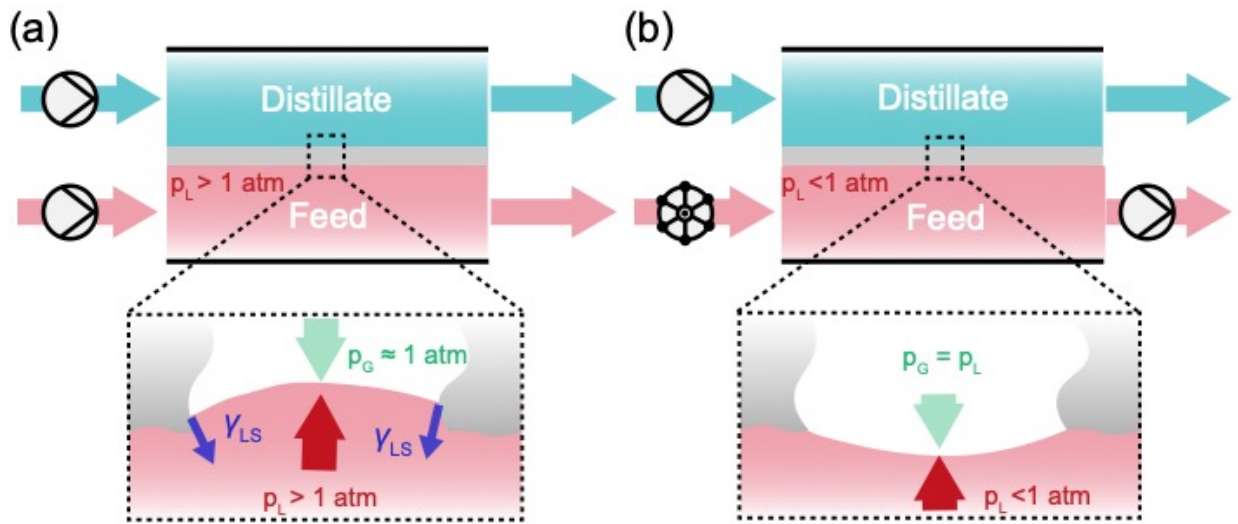
119 **MATERIALS AND METHOD**

120 **Membranes and chemicals** A commercial flat-sheet polyvinylidene fluoride (PVDF)
121 hydrophobic membrane (GVHP00010) was purchased from Millipore, USA. The PVDF
122 membrane has been extensively studied in the literature as a benchmark membrane and was fully
123 characterized (as listed in **Table S1**, mean pore size = 0.22 μm , thickness = 125 μm , water contact
124 angle = 110°, and liquid entry pressure (LEP) = 2.4 bar). Calcium chloride (CaCl_2 , analytical grade,
125 Sigma-Aldrich) and sodium sulfate (Na_2SO_4 , analytical grade, Sigma-Aldrich) were used as
126 received without further purification.

127 **Membrane distillation with positive and negative feed stream pressure** The MD
128 performance of the PVDF membrane under various operating conditions was evaluated using a
129 closed-loop bench-scale MD test unit. To avoid the influence of the pulse flow from the peristaltic
130 pump in the feed loop, a pressure buffer was placed at the inlet of the test cell. A gear pump was
131 used to circulate the distillate, and the conductivity of the distillate was constantly monitored using
132 a conductivity sensor. **Fig. 1a** and **b** schematically show the flow direction and the relative position
133 of the pump to create negative and positive gauge pressure in the feed channel of the MD cell.

134 For controlling the level of negative feed pressure, the feed pump was placed downstream of
135 the MD cell and an adjustable needle valve was used to change the inlet pressure (**Fig. 1b**). By
136 partially closing the valve, a higher degree of vacuum was created in the cell. To compensate for
137 flow rate reduction, the pumping speed was adjusted accordingly. The inlet pressure was
138 monitored using a digital pressure sensor (refer to **Fig. S1** for a schematic of the DCMD bench-
139 scale experimental setup). The difference between the pressures measured at the inlet and the outlet
140 of the MD cell is negligibly small, which suggests minimum pressure drop within the MD cell.
141 We note that the measured pressure outside the MD cell may not accurately reflect the actual

142 pressure inside the MD cell due to the Venturi effect. We have calculated the flow velocity within
 143 the feed and distillate channels based on their cross-sectional areas and used the Bernoulli equation
 144 to evaluate the pressure within the channels based on the pressure measured outside the cell. The
 145 calculation suggests that the difference between the pressures inside and outside the MD cell is
 146 negligibly small because velocity head is negligibly small as compared to the pressure head (**Table**
 147 **S2**).



148
 149 **Figure 1.** Schematic of DCMD with a **(a)** positive and **(b)** negative feed pressure. **(a)** With a
 150 positive feed pressure, the pump is placed upstream of the feed channel to push the solution into
 151 the feed channel. The local feed pressure is balanced by both the gas pressure in the pore and the
 152 interfacial force exerted by the pore edge. **(b)** With a negative feed pressure, the pump is placed
 153 downstream of the feed channel to pull the solution out of the feed channel. A valve is installed
 154 upstream of the cell so that both the flow rate and pressure can be controlled by adjusting the valve
 155 and the pump speed. The effective cell dimension was $50 \times 20 \times 3$ mm in length, width and height
 156 for both feed and distillate channels, respectively. The same feed and distillate flow velocity of
 157 0.17 m/s was maintained.

158 When a positive (gauge) pressure is applied on the feed stream ($P_L > 1$ atm), the feed pressure
 159 is balanced by both the gas pressure in the pore ($P_G > 1$ atm) the interfacial force (γ_{LS}) imposed by
 160 the hydrophobic membrane until liquid entry pressure is reached (**Fig. 1a**). Specifically, the force

161 balance can be described as $P_L - P_G = 2\gamma_{LS} / a$ with a being the pore radius. When a negative
162 (gauge) pressure is applied on the feed stream ($P_L < 1\text{atm}$), the interfacial force is negligible as the
163 liquid is not pushed into a hydrophobic pore, and the gas pressure within the pore is approximately
164 the same as the sub-atmospheric feed pressure (**Fig. 1b**).

165 If the feed pressure is only slightly negative, deformation of interface toward the feed solution
166 may increase the gas volume in the pore to account for the required vapor reduction, i.e., the pore
167 volume V must increase to decrease the total gas pressure P_G according to the ideal gas law
168 $P_G V = nRT$ (where n is the mole of gas in the pores, R is the ideal gas constant, and T is the
169 absolute temperature). However, the deformation of the liquid-gas interface can only occur to a
170 limited extent beyond which non-condensable gases in the pore must be partially removed (i.e., n
171 is reduced) via either dissolution into the feed stream or formation of gas bubbles to be carried
172 away by the flowing feed stream. In other words, the reduction of gas pressure within pores occurs
173 simply because the gas pressure must match the liquid pressure in the feed stream, which differs
174 from the mechanisms of gas pressure reduction in vacuum MD or air-gap MD.^{33, 34}

175 **Gypsum Scaling Experiments** A 1.2 L CaSO_4 feed solution (2000 mg/L, saturation
176 index=0.09) was prepared and pre-heated to 70 °C before the MD experiments.²³ The feed and
177 distillate streams flowed in a co-current mode. The water vapor flux across the membrane, J (L
178 $\text{m}^{-2} \text{h}^{-1}$), was monitored by measuring the distillate mass change over time. Experiments were
179 terminated at a flux decline of 50%. A feed spacer was used to promote turbulence and provide
180 mechanical support to the membrane. The spacer was 1.2 mm thick and was composed of filaments
181 with a diameter of 1 mm as schematically shown in **Fig. S2**.³⁵ In addition to performing
182 experiments using commercial PVDF membrane with both positive and negative pressure, we also

183 performed an additional experiment using superhydrophobic membrane with pulse flow, as it is
184 the state-of-the-art method of mitigating gypsum scaling and serves as a benchmark for
185 comparison. The fabrication of the superhydrophobic membrane using micropillar templating and
186 CF₄ plasma and the pulse flow operation were detailed in our previous publication (Supporting
187 Information **S1.4** and **S1.5**).²³

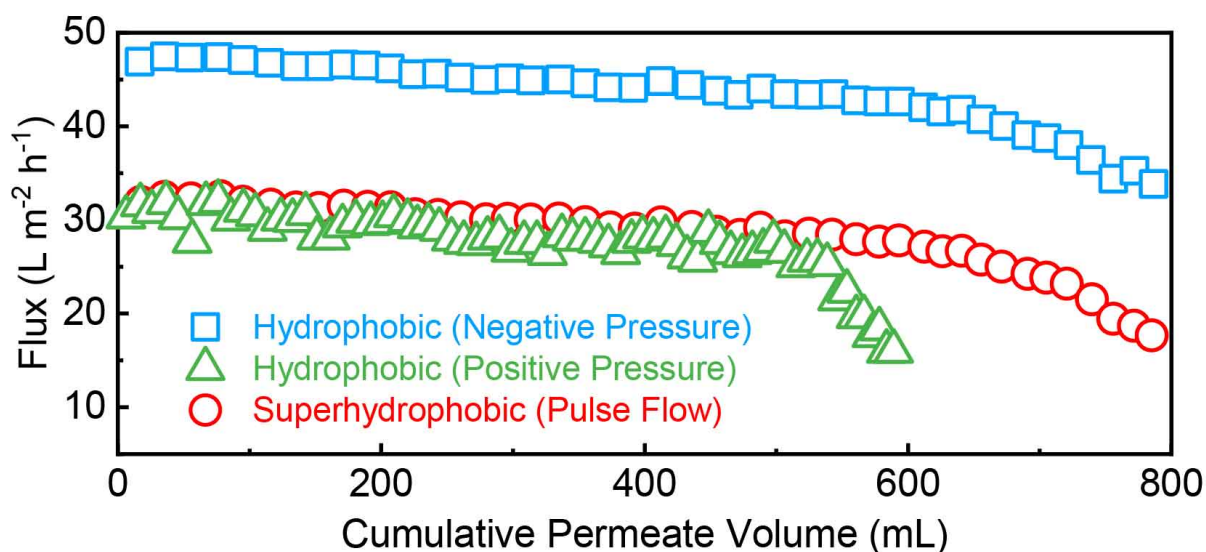
188 To identify the scalants on the membrane surfaces, the scaled membrane samples were
189 taken out of the test cell, rinsed with deionized water to remove excess feed solution, and dried
190 (the CaSO₄ precipitates adhered strongly enough to the membrane and were thus not removed by
191 a gentle rinse). The dried membrane with scalant on surface was sputter-coated with a thin layer
192 of gold and analyzed via scanning electron microscopy (HITACH TM-1000).

193

194 **RESULTS AND DISCUSSION**

195 **Membrane wetting properties** The commercial PVDF membrane exhibited a water contact
196 angle of 110°, but no sliding angle was measured as the drop stayed pinned even on a vertical
197 surface (**Table S1**). Thus, under zero and positive gauge pressure, liquid intrudes into the
198 membrane pores and the PVDF membrane surface is partially wetted (i.e., the liquid-gas interface
199 is within the pores).³⁶ Constrained by the pump specifications, the negative feed pressure was
200 limited to a minimum gauge pressure of -30.0 kPa (-0.3 bar), which was far below the liquid entry
201 pressure (LEP) of the PVDF membrane (2.4 bar, **Table S1**) and thus would not induce penetration
202 of distillate into the membrane pores. In all the scaling experiments to be discussed below, the
203 distillate conductivity was $\sim 10 \pm 1$ $\mu\text{S}/\text{cm}$, which suggests the absence of pore wetting.

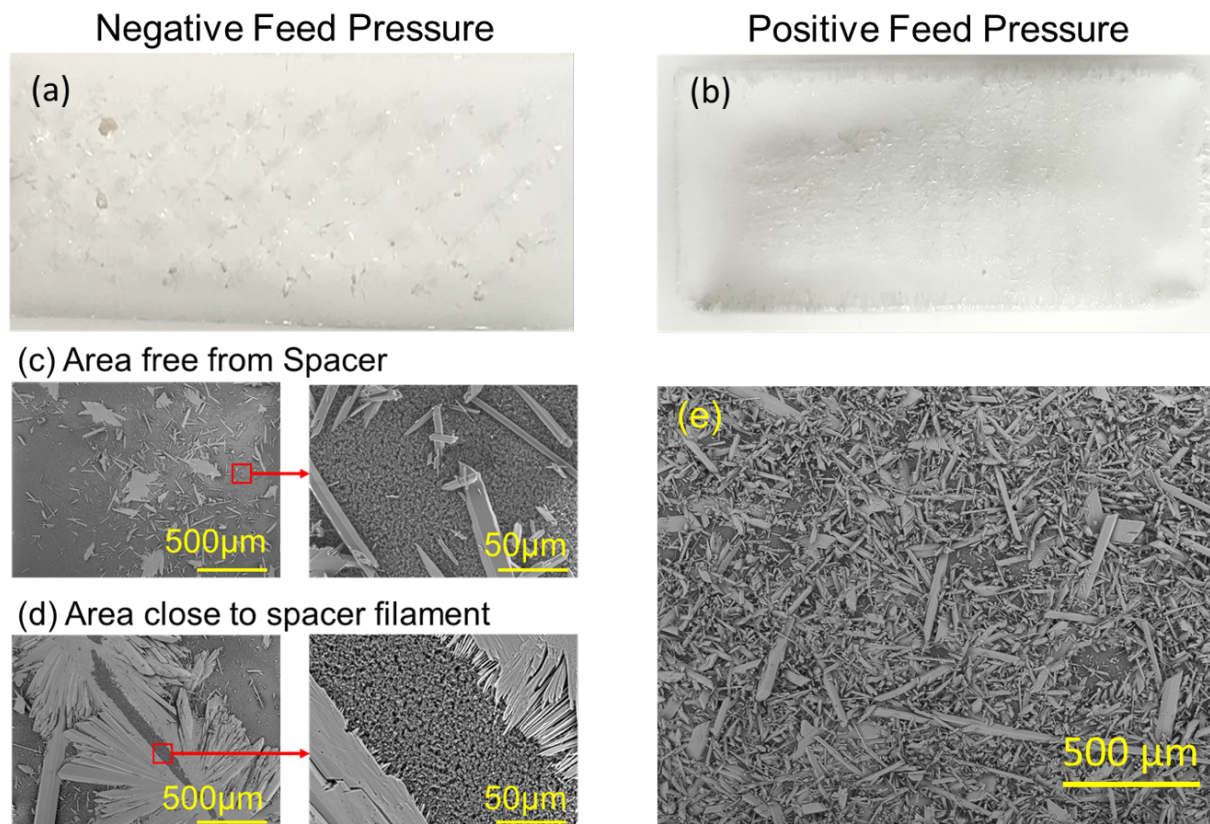
204 **Scaling resistance with negative feed pressure** At a positive feed pressure of 1.0 kPa, the
 205 flux of the PVDF membrane quickly declined after 500 mL of distillate was recovered from the
 206 feed solution (**Fig. 2**, green triangles), indicating the onset of precipitous gypsum nucleation and
 207 deposition of gypsum crystals that blocked the membrane pores. When a superhydrophobic
 208 membrane was used in combination with pulse flow, flux decline was substantially slower after
 209 recovering 500 mL of distillate (**Fig. 2**, red circles). This slow flux decline indicates insignificant
 210 gypsum scaling, which has been elaborated in our previous study with the support of scanning
 211 electron microscopy (SEM) images showing the absence of precipitate on the membrane surface²³.
 212 We showed in same study that neither superhydrophobic membrane nor pulse flow alone could
 213 achieve resistance to gypsum scaling, and that the synergy between the two factors is critical.²³



214
 215 **Figure 2.** Scaling resistance (to gypsum as the scalant) of commercial hydrophobic membrane
 216 under positive pressure (green triangles, 1.0 kPa), under negative pressure (blue squares, -30.0
 217 kPa), and superhydrophobic (slippery) membrane with pulse flow operation (red circles).²³ The
 218 feed solution contained 2000 mg L⁻¹ CaSO₄ solution (saturation index, SI=0.09). The temperatures
 219 of the feed solution and distillate were 70 °C and 20 °C, respectively. The same crossflow velocity
 220 of 0.17 m/s was used in both the feed and distillate streams. The experiments were stopped when
 221 the cumulative distillate volume reached 800 mL because the feed volume became insufficient for
 222 flow circulation. (Reproductive experimental data are in the Supporting Information **Fig. S3**)

223 In this study, we observe that the same excellent resistance to gypsum scaling, as achieved
224 using superhydrophobic membrane with pulse flow, can also be achieved with a conventional
225 hydrophobic membrane and a negative feed pressure of -30.0 kPa (**Fig. 2**, Blue squares). Even
226 with a cumulative distillate volume of 800 mL (corresponding to a water recovery over 66%), only
227 a small degree of gradual flux decline was observed possibly due to the reduction of partial vapor
228 pressure at high salinity. At this water recovery, the CaSO₄ concentration in the feed solution was
229 above 5000 mg L⁻¹ (SI = 0.48) and the solution was far beyond saturation. Surprisingly, the vapor
230 flux was ~60% higher with operation using negative gauge pressure than that using positive gauge
231 pressure, which will be elucidated in more detail in the following section.

232 At negative feed pressure, the majority of CaSO₄ crystals on the PVDF membrane formed
233 in the regions contacting the spacer (**Fig. 3a,c,d**). Accumulation of crystals next to the spacer
234 filament (**Fig. 3d**) was likely due to the presence of hydrodynamically stagnant regions that favor
235 (1) deposition of mineral precipitates,^{37, 38} and (2) more severe concentration polarization that
236 facilitates nucleation and crystal growth.^{39, 40} Far from the spacer filament (**Fig. 3c**), where
237 negative feed pressure has greater influence on the shape and position of the liquid-gas interface,
238 significantly fewer crystal precipitates were observed. In contrast, the PVDF membrane operated
239 at positive feed pressure of 1.0 kPa was fully covered with CaSO₄ crystals (**Fig. 3b,e**). These
240 observations confirm the results (e.g., flux decline) from the DCMD experiments, that the novel
241 operating strategy using negative feed pressure can effectively mitigate membrane scaling (by
242 gypsum) even if only a commercial hydrophobic membrane is used.

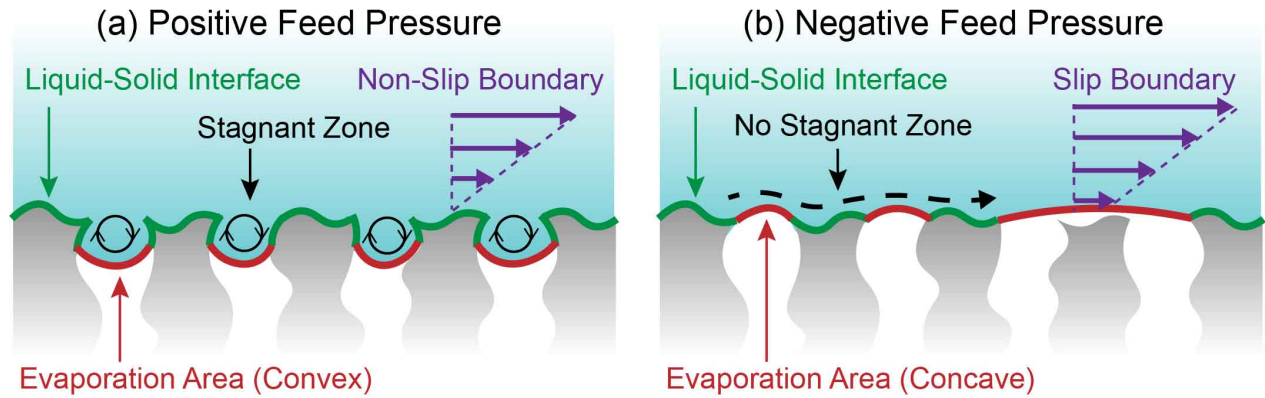


243

244 **Figure 3.** Photographic images of the membrane surface after experiments of (a) NP-DCMD and
 245 (b) conventional DCMD. SEM images of the membrane surface after experiments of (c, d) NP-
 246 DCMD and (e) conventional DCMD. Specifically, panel (c) shows the area uncovered by the
 247 spacer filament and panel (d) shows the area covered by or near to the spacer filament. All
 248 photographic and SEM images were obtained using commercial hydrophobic membrane (C-
 249 PVDF).

250 The excellent scaling resistance observed with negative feed pressure on a commercial
 251 hydrophobic membrane can be attributed to the influence of the negative feed pressure on the
 252 shape and position of the liquid-gas interface (**Fig. 4**). In conventional DCMD with a hydrophobic
 253 membrane and a positive feed pressure, the meniscus (i.e., the liquid-gas interface) is convex and
 254 the membrane pores are partially wetted near the pore mouths (**Fig. 4a**). This partial intrusion of
 255 feed solution, along with the non-slip boundary condition, creates hydrodynamically stagnant
 256 zones in the pores near the membrane surface. These stagnant zones exacerbate concentration
 257 polarization and increase the residence time for crystal deposition and growth. When a negative

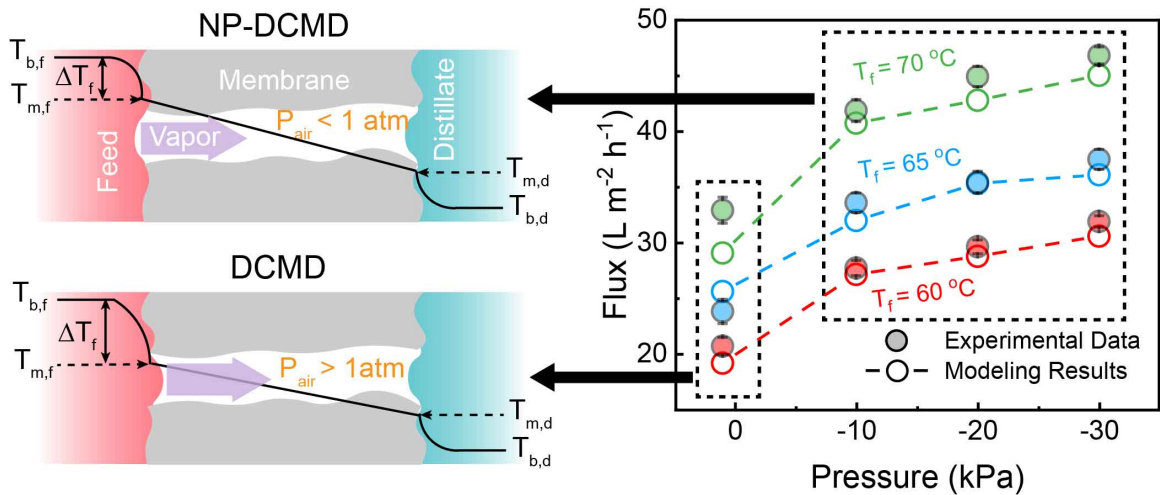
258 feed pressure is applied, however, these stagnant zones and the non-slip boundary conditions no
259 longer exist, as the liquid-gas interface becomes concave and curved into the feed solution (**Fig.**
260 **4b**).



261
262 **Figure 4.** Schematic illustration of the proposed mechanisms for the scaling resistance and
263 enhanced flux. **(a)** With a positive feed pressure, the meniscus (i.e., the water-air interface) is
264 convex, the area for water-membrane contact is larger, the flow of the feed stream has a non-slip
265 boundary condition and there are stagnant zones at the entrance of the pores. **(b)** With a negative
266 feed pressure, the meniscus is concave, the area for water-membrane contact is smaller, the flow
267 of the feed stream has a slip boundary condition and there is no stagnant zone near the membrane
268 surface.

269 The scaling resistance imparted by the concave liquid-gas interface has two possible
270 mechanisms: (1) the concave liquid-gas interface reduces the liquid-membrane contact area
271 available for crystal adhesion and growth; (2) the concave liquid-gas interface introduces a slip
272 boundary condition at the feed solution-membrane interface, which mitigates concentration
273 polarization and decreases the residence time for crystal deposition and growth.^{11, 41} Both effects
274 possibly have contributed to the scaling resistance of a superhydrophobic membrane (in regular
275 MD) that reduces the convexity of the water-air interface and minimizes the liquid intrusion into
276 pores. But the concave interface and the complete elimination of pore intrusion in NP-DCMD with
277 hydrophobic membranes are likely even more effective in mitigating mineral scaling than regular
278 DCMD with superhydrophobic membranes .

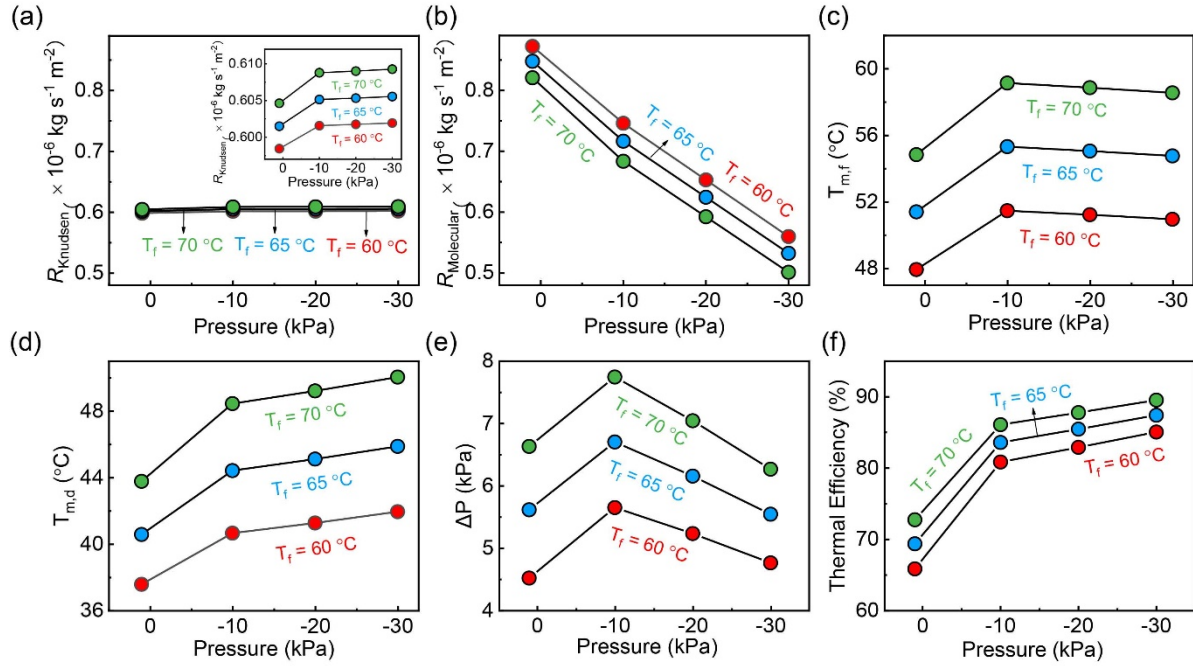
279 **Flux enhancement with negative feed pressure** The initial flux of negative pressure direct
 280 contact membrane distillation (NP-DCMD) was $48.6 \text{ L m}^{-2} \text{ h}^{-1}$, which was 62 % higher than that
 281 of conventional DCMD under positive pressure (**Fig. 2**). To better understand this remarkable flux
 282 enhancement, the NP-DCMD vapor flux was measured experimentally over a range of feed
 283 pressures and temperatures (**Fig. 5**). Water vapor flux increased with decreasing feed pressure at
 284 any given feed temperature. Increasing temperature resulted in a nonlinear increase in water vapor
 285 flux due to the exponential dependence of water vapor pressure on temperature. We estimated the
 286 vapor flux for NP-DCMD using the Dusty-Gas model by considering the effects of temperature
 287 and pressure on: (1) molecular diffusion resistance, which influenced the membrane permeability
 288 coefficient, and (2) the heat transfer, which influences the temperature profile, and thus, the partial
 289 vapor pressure across the membrane.
 290



291
 292 **Figure. 5 Left:** Schematic illustration of temperature distribution T and air pressure in the pores
 293 P_{air} in both of DCMD and NP-DCMD. The subscript b, m, f and d of T denote the bulk, membrane
 294 surface, feed and distillate side, respectively. **Right:** Vapor flux as functions of feed gauge pressure
 295 (1.0 kPa to -30.0 kPa) at 60°C (red), 65°C (blue) and 70°C (green), respectively. The filled circles
 296 represent the experimental data whereas the empty circles represent the simulated results based on
 297 the Dusty-Gas model (shown in **Section S4: MATLAB code of mass and heat transfer in NP-**
 298 **DCMD**). The error bar of experimental results was shown in **Table S3**.

299
300
301
302
303
304
305
306
307
308
309
310
311
312
313
314

To quantify the effect of pore air pressure on vapor transfer resistance, we considered the Knudsen flow and molecular diffusion resistances, which are the two major resistances of vapor transfer through membrane pores in DCMD (model derivations are presented in **Section S2: Vapor transport in MD**).¹ The Knudsen resistance increases negligibly with feed pressure and temperature due to the slight increase in the average membrane pore temperature with decreasing feed pressure (**Eq. S2.1, Fig. 6a**). However, the molecular diffusion resistance decreases dramatically as feed pressure decreases because the negative feed pressure directly reduces the air pressure inside the membrane pores (**Eq. S2.2, Fig. 6b**), which increases the membrane permeability coefficient, and thus, increases the water vapor flux. In fact, in vacuum enhanced DCMD, where negative gauge pressure is applied to the distillate stream, a similar mechanism for flux enhancement has been proposed.⁴² However, the magnitude of flux enhancement predicted based on changes of Knudsen and molecular diffusion resistances is significantly and consistently less than experimental observations (**Fig. S4**), which suggests that the impact of negative pressure on enhanced vapor transport alone is insufficient to explain the observed flux enhancement.



315

316 **Figure 6.** (a) Resistance for Knudsen diffusion. (b) Resistance for molecular diffusion. (c)
 317 Temperature at membrane surface contacting the feed stream. (d) Temperature at membrane
 318 surface contacting the distillate stream. (e) Water vapor pressure difference across the pores of an
 319 MD membrane. (f) Thermal efficiency. All parameters are evaluated for four different feed gauge
 320 pressures, including positive (1.0 kPa) and negative (-10, -20 and -30 kPa) pressures, and for three
 321 feed bulk temperatures (60, 65 and 70 °C) with distillate bulk temperature maintained at 20 °C.

322 Next, the effect of heat transfer on water vapor flux with negative feed pressure was considered.

323 The liquid-gas interface on the feed side of the membrane is convex with a positive feed pressure

324 and concave with a negative feed pressure. The slip boundary induced by the concave meniscus

325 in NP-DCMD results in a larger convective heat transfer coefficient, h_f , relative to that in a

326 regular DCMD process. The enhanced convective heat transfer reduces the feed side temperature

327 polarization and increases the local temperature at the feed solution/membrane interface (Eq.

328 S3.2, Fig. 6c).⁴³ The concave meniscus also reduces the liquid-solid interfacial area while

329 increasing the liquid-gas interfacial area available for evaporation, decreasing overall conductive

330 heat transfer coefficient of the membrane, h_m (Eq. S3.4). To account for these differences in heat

331 transfer in NP-DCMD, h_f was multiplied by a correction factor ϕ_1 which accounts for the

332 enhanced hydrodynamics in the boundary layer, and h_m was multiplied by a correction factor φ_2
333 which accounts for the impact of concave meniscus on conductive heat transfer. In conventional
334 DCMD with positive feed pressure, φ_1 and φ_2 are taken to be unity (i.e., no correction is applied)
335 and the heat transfer coefficients are extracted from fitting the experimental data. Using the same
336 set of parameters extracted from conventional DCMD (except φ_1 and φ_2), we find that $\varphi_1 = 1.7$
337 and $\varphi_2 = 0.7$ when a negative feed pressure was applied (More information could be found in
338 **Section 3: Detailed description of heat transfer in MD**).

339 Heat transfer has a direct impact on the driving force for vapor transfer. The slip boundary
340 condition and the reduced trans-membrane conductive heat transfer, both resulting from the
341 concave liquid-gas interface, contribute to reduced temperature polarization in the feed stream and
342 affect the temperature at the feed/membrane interface, $T_{m,f}$ (**Fig. 6c**), and that at the
343 distillate/membrane interface, $T_{m,d}$ (**Fig. 6d**). The changes in $T_{m,f}$ and $T_{m,d}$ result in the change
344 of vapor pressure difference which is the driving force for vapor transfer (**Fig. 6e**). While the
345 calculated change of driving force with more negative feed pressure is not monotonic, the observed
346 monotonic increase in flux (**Fig. 5**) is a result of both non-monotonic variation in driving force and
347 monotonic reduction in vapor transfer resistance. Considering both the impacts of negative
348 pressure on the trans-membrane vapor pressure difference (**Fig. 6e**) and the vapor transport
349 resistances (**Fig. 6a,b**), the revised mass transfer transfer for NP-DCMD can accurately explain
350 the experimentally observed flux enhancement (**Fig. 5**).

351 Lastly, the enhanced vapor flux and reduced conductive heat transfer due to negative feed
352 pressure result in a higher thermal efficiency (**Fig. 6f**), i.e., more efficient utilization of driving
353 force for vapor transfer. In other words, NP-DCMD also has extra kinetic (i.e., high vapor flux)

354 and energetic (i.e., higher energy efficiency) benefits in addition to the exceptional scaling
355 resistance. The thermal efficiency achieved using NP-DCMD with a commercial hydrophobic
356 membrane is among the highest in all DCMD processes reported in literature.^{44, 45}

357

358 **IMPLICATIONS**

359 Instead of resorting to complicated membrane design based on multi-step surface
360 modifications with chemical or/and physical approaches, our study demonstrates a much simpler
361 and practically more appealing approach of scaling mitigation using the novel operation strategy
362 of NP-DCMD which also offers the additional benefit of substantial enhancement of flux and
363 thermal efficiency. The very effective scaling mitigation achieved by NP-DCMD may potentially
364 enable MD to push the limit of water recovery for brine volume minimization or even zero liquid
365 discharge. To reach that goal, more work needs to be performed to understand the effectiveness of
366 NP-DCMD in mitigating other types of scaling, particularly when it is challenged with real feed
367 water with a complex composition.^{46, 47} In addition, the effectiveness of NP-DCMD for scaling
368 mitigation should also be benchmarked against that of using antiscalants. The combination of NP-
369 DCMD and antiscalants is also worthy of investigation. Moreover, while we can easily control the
370 pressure in a bench-scale system, pressure drop along a full-scale MD module will result in spatial
371 distribution of feed pressure and effectiveness of scaling mitigation. Future research to address
372 these unexplored aspects will further advance NP-DCMD to become potentially the most effective
373 approach for addressing scaling which is arguably the most critical challenge in MD for high-
374 salinity and high-recovery applications.

375 **ASSOCIATED CONTENT**

376 **Supporting Information**

377 Experimental details for membrane characterization and performance test (S1), Vapor transport in
378 MD (S2), Detailed description of heat transfer in MD (S3), MATLAB code of mass and heat
379 transfer in NP-DCMD (S4), Characteristics of the commercial PVDF and CF₄-MP-PVDF (Table
380 S1), The pressures measured outside the tube and the pressures in the feed channel calculated based
381 on Bernoulli equation (Table S2), Mean value (and standard deviation) water flux under different
382 temperature and pressures (Table S3), Schematic and photographic image and of the DCMD
383 experimental setup (Fig. S1), Schematic illustration of the spacer structure (Fig. S2), Replicate
384 data of NP-DCMD experiment with a feed solution containing 2000 ppm CaSO₄ (Fig. S3),
385 Simulation results without considering the heat transfer (Fig. S4)

386

387 **ACKNOWLEDGMENT**

388 The research was partially supported by National Natural Science Foundation of China (No.
389 21978315, 52011530031), Newton Advanced Fellowship from Royal Society (No. NA170113),
390 CAS International Collaboration (No. GJHZ2080) and US National Science Foundation (No.
391 1903685). We also thank the frame work research consortium for partially financial support
392 (RFBR No. 18-58-80031, NSFC No. 51861145313, DST IPN/7864, NRT No.116020,
393 CNPq/BRICS-STI-2-442229/2017-8).

394

395 **REFERENCES**

- 396 1. Alkhudhiri, A.; Darwish, N.; Hilal, N., Membrane distillation: A comprehensive review. *Desalination*
397 **2012**, *287*, 2-18.
- 398 2. Tong, T.; Elimelech, M., The Global Rise of Zero Liquid Discharge for Wastewater Management:
399 Drivers, Technologies, and Future Directions. *Environmental Science & Technology* **2016**, *50*, (13), 6846-
400 55.
- 401 3. Deshmukh, A.; Boo, C.; Karanikola, V.; Lin, S.; Straub, A. P.; Tong, T.; Warsinger, D. M.; Elimelech,
402 M., Membrane distillation at the water-energy nexus: limits, opportunities, and challenges. *Energy &*
403 *Environmental Science* **2018**, *11*, (5), 1177-1196.
- 404 4. Ghaffour, N.; Soukane, S.; Lee, J. G.; Kim, Y.; Alpatova, A., Membrane distillation hybrids for water
405 production and energy efficiency enhancement: A critical review. *Applied Energy* **2019**, *254*, 113698.
- 406 5. Naidu, G.; Jeong, S.; Vigneswaran, S.; Hwang, T.-M.; Choi, Y.-J.; Kim, S.-H., A review on fouling of
407 membrane distillation. *Desalin. Water Treat.* **2015**, *57*, (22), 10052-10076.
- 408 6. Warsinger, D. M.; Swaminathan, J.; Guillen-Burrieza, E.; Arafat, H. A.; Lienhard V, J. H., Scaling and
409 fouling in membrane distillation for desalination applications: A review. *Desalination* **2015**, *356*, 294-313.
- 410 7. Liu, L.; Xiao, Z.; Liu, Y.; Li, X.; Yin, H.; Volkov, A.; He, T., Understanding the fouling/scaling resistance
411 of superhydrophobic/omniphobic membranes in membrane distillation. *Desalination* **2021**, *499*, 114864.
- 412 8. Karanikola, V.; Boo, C.; Rolf, J.; Elimelech, M., Engineered Slippery Surface to Mitigate Gypsum
413 Scaling in Membrane Distillation for Treatment of Hypersaline Industrial Wastewaters. *Environmental*
414 *Science & Technology* **2018**, *52*, (24), 14362-14370.
- 415 9. Bush, J. A.; Vanneste, J.; Gustafson, E. M.; Waechter, C. A.; Jassby, D.; Turchi, C. S.; Cath, T. Y.,
416 Prevention and management of silica scaling in membrane distillation using pH adjustment. *J. Membr. Sci.*
417 **2018**, *554*, 366-377.
- 418 10. Curcio, E.; Ji, X.; Di Profio, G.; Sulaiman, A. O.; Fontananova, E.; Drioli, E., Membrane distillation
419 operated at high seawater concentration factors: Role of the membrane on CaCO₃ scaling in presence of
420 humic acid. *J. Membr. Sci.* **2010**, *346*, (2), 263-269.
- 421 11. Xiao, Z.; Zheng, R.; Liu, Y.; He, H.; Yuan, X.; Ji, Y.; Li, D.; Yin, H.; Zhang, Y.; Li, X. M.; He, T., Slippery
422 for scaling resistance in membrane distillation: A novel porous micropillared superhydrophobic surface.
423 *Water Res* **2019**, *155*, 152-161.
- 424 12. Mericq, J. P.; Laborie, S.; Cabassud, C., Vacuum membrane distillation of seawater reverse osmosis
425 brines. *Water Res* **2010**, *44*, (18), 5260-73.
- 426 13. Lim, J.; Son, K. P.; Kang, S. M.; Park, J.; Min, S.; Cho, H.; Kim, S.-H.; Lee, S.; Chae, S.; Park, P.-K.,
427 Correlation between the feed composition and membrane wetting in a direct contact membrane
428 distillation process. *Environmental Science: Water Research & Technology* **2021**, *7*, (6), 1020-1031.
- 429 14. Christie, K. S. S.; Yin, Y.; Lin, S.; Tong, T., Distinct Behaviors between Gypsum and Silica Scaling in
430 Membrane Distillation. *Environmental Science & Technology* **2020**, *54*, (1), 568-576.
- 431 15. Su, C.; Horseman, T.; Cao, H.; Christie, K.; Li, Y.; Lin, S., Robust Superhydrophobic Membrane for
432 Membrane Distillation with Excellent Scaling Resistance. *Environmental Science & Technology* **2019**, *53*,
433 (20), 11801-11809.
- 434 16. Tong, T.; Wallace, A. F.; Zhao, S.; Wang, Z., Mineral scaling in membrane desalination: Mechanisms,
435 mitigation strategies, and feasibility of scaling-resistant membranes. *J. Membr. Sci.* **2019**, *579*, 52-69.
- 436 17. Horseman, T.; Yin, Y.; Christie, K. S. S.; Wang, Z.; Tong, T.; Lin, S., Wetting, Scaling, and Fouling in
437 Membrane Distillation: State-of-the-Art Insights on Fundamental Mechanisms and Mitigation Strategies.
438 *ACS ES&T Engineering* **2020**, *1*, (1), 117-140.
- 439 18. Xiao, Z.; Li, Z.; Guo, H.; Liu, Y.; Wang, Y.; Yin, H.; Li, X.; Song, J.; Nghiem, L. D.; He, T., Scaling
440 mitigation in membrane distillation: From superhydrophobic to slippery. *Desalination* **2019**, *466*, 36-43.
- 441 19. Lin, S.; Nejati, S.; Boo, C.; Hu, Y.; Osuji, C. O.; Elimelech, M., Omniphobic Membrane for Robust
442 Membrane Distillation. *Environ. Sci. Technol. Lett.* **2014**, *1*, (11), 443-447.

- 443 20. Boo, C.; Lee, J.; Elimelech, M., Omniphobic Polyvinylidene Fluoride (PVDF) Membrane for
444 Desalination of Shale Gas Produced Water by Membrane Distillation. *Environmental Science & Technology*
445 **2016**, *50*, (22), 12275-12282.
- 446 21. Chen, L.-H.; Huang, A.; Chen, Y.-R.; Chen, C.-H.; Hsu, C.-C.; Tsai, F.-Y.; Tung, K.-L., Omniphobic
447 membranes for direct contact membrane distillation: Effective deposition of zinc oxide nanoparticles.
448 *Desalination* **2018**, *428*, 255-263.
- 449 22. Chen, Y.; Lu, K. J.; Chung, T.-S., An omniphobic slippery membrane with simultaneous anti-wetting
450 and anti-scaling properties for robust membrane distillation. *J. Membr. Sci.* **2020**, *595*, 117572.
- 451 23. Liu, Y.; Li, Z.; Xiao, Z.; Yin, H.; Li, X.; He, T., Synergy of slippery surface and pulse flow: An anti-
452 scaling solution for direct contact membrane distillation. *J. Membr. Sci.* **2020**, *603*, 118035.
- 453 24. Horseman, T.; Su, C.; Christie, K. S. S.; Lin, S., Highly Effective Scaling Mitigation in Membrane
454 Distillation Using a Superhydrophobic Membrane with Gas Purging. *Environ. Sci. Technol. Lett.* **2019**, *6*, (7),
455 423-429.
- 456 25. Robbins, C. A.; Grauberger, B. M.; Garland, S. D.; Carlson, K. H.; Lin, S.; Bandhauer, T. M.; Tong, T.,
457 On-site treatment capacity of membrane distillation powered by waste heat or natural gas for
458 unconventional oil and gas wastewater in the Denver-Julesburg Basin. *Environ Int* **2020**, *145*, 106142.
- 459 26. Lohmann, R.; Cousins, I. T.; DeWitt, J. C.; Gluge, J.; Goldenman, G.; Herzke, D.; Lindstrom, A. B.;
460 Miller, M. F.; Ng, C. A.; Patton, S.; Scheringer, M.; Trier, X.; Wang, Z., Are Fluoropolymers Really of Low
461 Concern for Human and Environmental Health and Separate from Other PFAS? *Environmental Science &*
462 *Technology* **2020**, *54*, (20), 12820-12828.
- 463 27. Razmjou, A.; Arifin, E.; Dong, G.; Mansouri, J.; Chen, V., Superhydrophobic modification of TiO₂
464 nanocomposite PVDF membranes for applications in membrane distillation. *J. Membr. Sci.* **2012**, *415-416*,
465 850-863.
- 466 28. Lee, E.-J.; An, A. K.; He, T.; Woo, Y. C.; Shon, H. K., Electrospun nanofiber membranes incorporating
467 fluorosilane-coated TiO₂ nanocomposite for direct contact membrane distillation. *J. Membr. Sci.* **2016**,
468 *520*, 145-154.
- 469 29. Zhang, H.; Li, B.; Sun, D.; Miao, X.; Gu, Y., SiO₂-PDMS-PVDF hollow fiber membrane with high flux
470 for vacuum membrane distillation. *Desalination* **2018**, *429*, 33-43.
- 471 30. Efome, J. E.; Baghbanzadeh, M.; Rana, D.; Matsuura, T.; Lan, C. Q., Effects of superhydrophobic
472 SiO₂ nanoparticles on the performance of PVDF flat sheet membranes for vacuum membrane distillation.
473 *Desalination* **2015**, *373*, 47-57.
- 474 31. Zheng, R.; Chen, Y.; Wang, J.; Song, J.; Li, X.-M.; He, T., Preparation of omniphobic PVDF membrane
475 with hierarchical structure for treating saline oily wastewater using direct contact membrane distillation.
476 *J. Membr. Sci.* **2018**, *555*, 197-205.
- 477 32. Wang, W.; Du, X.; Vahabi, H.; Zhao, S.; Yin, Y.; Kota, A. K.; Tong, T., Trade-off in membrane
478 distillation with monolithic omniphobic membranes. *Nat Commun* **2019**, *10*, (1), 3220.
- 479 33. Alsaadi, A. S.; Alpatova, A.; Lee, J.-G.; Francis, L.; Ghaffour, N., Flashed-feed VMD configuration as
480 a novel method for eliminating temperature polarization effect and enhancing water vapor flux. *J. Membr.*
481 *Sci.* **2018**, *563*, 175-182.
- 482 34. Alsaadi, A. S.; Francis, L.; Maab, H.; Amy, G. L.; Ghaffour, N., Evaluation of air gap membrane
483 distillation process running under sub-atmospheric conditions: Experimental and simulation studies. *J.*
484 *Membr. Sci.* **2015**, *489*, 73-80.
- 485 35. Yang, C.; Tian, M.; Xie, Y.; Li, X.-M.; Zhao, B.; He, T.; Liu, J., Effective evaporation of CF₄ plasma
486 modified PVDF membranes in direct contact membrane distillation. *J. Membr. Sci.* **2015**, *482*, 25-32.
- 487 36. Nagayama, G.; Zhang, D., Intermediate wetting state at nano/microstructured surfaces. *Soft*
488 *Matter* **2020**, *16*, (14), 3514-3521.
- 489 37. Al-Sharif, S.; Albeirutty, M.; Cipollina, A.; Micale, G., Modelling flow and heat transfer in spacer-
490 filled membrane distillation channels using open source CFD code. *Desalination* **2013**, *311*, 103-112.

491 38. Haidari, A. H.; Heijman, S. G. J.; van der Meer, W. G. J., Optimal design of spacers in reverse
 492 osmosis. *Separation and Purification Technology* **2018**, *192*, 441-456.

493 39. Fane, A. G.; Beatson, P.; Li, H., Membrane fouling and its control in environmental applications.
 494 *Water Sci. Technol.* **2000**, *41*, (10-11), 303-308.

495 40. Thomas, N.; Sreedhar, N.; Al-Ketan, O.; Rowshan, R.; Abu Al-Rub, R. K.; Arafat, H., 3D printed
 496 spacers based on TPMS architectures for scaling control in membrane distillation. *J. Membr. Sci.* **2019**,
 497 *581*, 38-49.

498 41. Warsinger, D. M.; Tow, E. W.; Swaminathan, J.; Lienhard V, J. H., Theoretical framework for
 499 predicting inorganic fouling in membrane distillation and experimental validation with calcium sulfate. *J.*
 500 *Membr. Sci.* **2017**, *528*, 381-390.

501 42. Cath, T. Y.; Adams, V. D.; Childress, A. E. Vacuum enhanced direct contact membrane distillation.
 502 US 7,608,188 B2, 2009.

503 43. Enright, R.; Hodes, M.; Salamon, T.; Muzychka, Y., Isoflux Nusselt Number and Slip Length
 504 Formulae for Superhydrophobic Microchannels. *Journal of Heat Transfer* **2014**, *136*, (1), 012402.

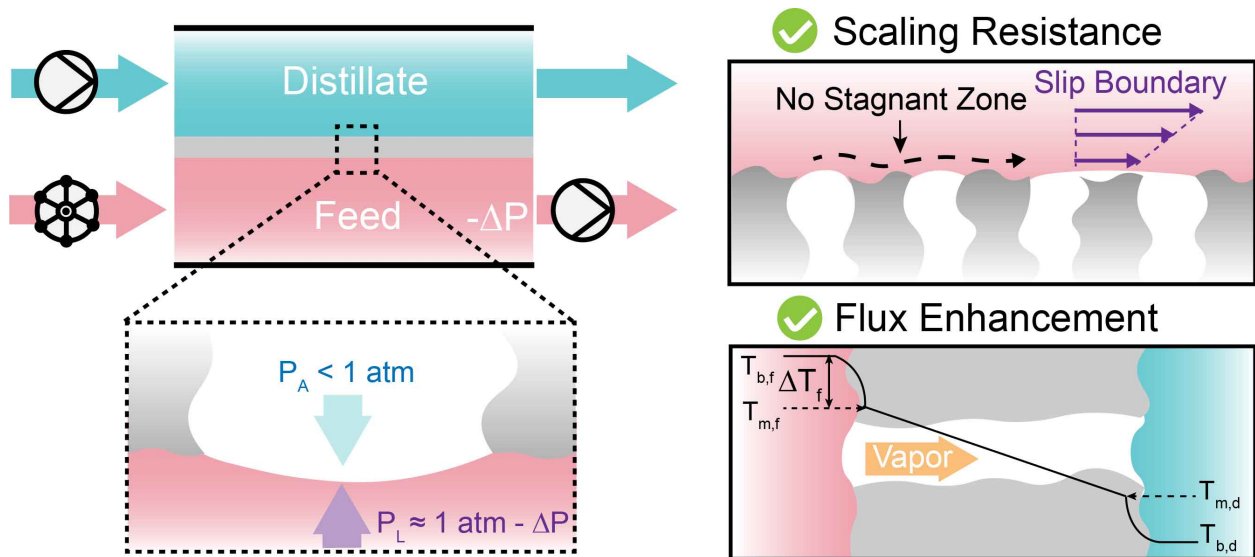
505 44. Zhang, Y.; Peng, Y.; Ji, S.; Li, Z.; Chen, P., Review of thermal efficiency and heat recycling in
 506 membrane distillation processes. *Desalination* **2015**, *367*, 223-239.

507 45. Leitch, M. E.; Li, C.; Ikkala, O.; Mauter, M. S.; Lowry, G. V., Bacterial Nanocellulose Aerogel
 508 Membranes: Novel High-Porosity Materials for Membrane Distillation. *Environ. Sci. Technol. Lett.* **2016**, *3*,
 509 (3), 85-91.

510 46. Lee, J.-G.; Jang, Y.; Fortunato, L.; Jeong, S.; Lee, S.; Leiknes, T.; Ghaffour, N., An advanced online
 511 monitoring approach to study the scaling behavior in direct contact membrane distillation. *J. Membr. Sci.*
 512 **2018**, *546*, 50-60.

513 47. Fortunato, L.; Jang, Y.; Lee, J.-G.; Jeong, S.; Lee, S.; Leiknes, T.; Ghaffour, N., Fouling development
 514 in direct contact membrane distillation: Non-invasive monitoring and destructive analysis. *Water research*
 515 **2018**, *132*, 34-41.

516 **TOC**



517